

Hybrid-RRAM towards next generation of non-volatile memory: Coupling of oxygen vacancies and metal ions

Gilbert Sassine, Cecile Nail, Philippe Blaise, Benoit Sklenard, Mathieu Bernard, Rémy Gassilloud, Aurélie Marty, Marc Veillerot, Christophe Vallee, Etienne Nowak, et al.

▶ **To cite this version:**

Gilbert Sassine, Cecile Nail, Philippe Blaise, Benoit Sklenard, Mathieu Bernard, et al.. Hybrid-RRAM towards next generation of non-volatile memory: Coupling of oxygen vacancies and metal ions. Advanced Electronic Materials, 2018, 5 (2), pp.1800658. 10.1002/aelm.201800658 . cea-02885888

HAL Id: cea-02885888
https://cea.hal.science/cea-02885888

Submitted on 1 Jul 2020

HAL is a multi-disciplinary open access archive for the deposit and dissemination of scientific research documents, whether they are published or not. The documents may come from teaching and research institutions in France or abroad, or from public or private research centers.

L'archive ouverte pluridisciplinaire **HAL**, est destinée au dépôt et à la diffusion de documents scientifiques de niveau recherche, publiés ou non, émanant des établissements d'enseignement et de recherche français ou étrangers, des laboratoires publics ou privés.

DOI: 10.1002/ ((please add manuscript number))
Article type: Full Paper

Title Hybrid-RRAM Towards Next Generation of Non-volatile Memory: Coupling of Oxygen Vacancies and Metal Ions

Author(s), and Corresponding Author(s) Gilbert Sassine*, Cécile Nail, Philippe Blaise, Benoit Sklenard, Mathieu Bernard, Rémy Gassilloud, Aurélie Marty, Marc Veillerot, Christophe Vallée, Etienne Nowak, and Gabriel Molas**

G. S., C. N., P. B., B. S., M. B., R. G., A. M., M. V., E.N., G.M.
CEA LETI Minatec Campus, 17 avenue des Martyrs, 38045 Grenoble, France
E-mail: gilbert.sassine@cea.fr, Gabriel.molas@cea.fr

C. V.
LTM CNRS, 17 avenue des Martyrs, 38045 Grenoble, France

Keywords: hybrid rram, reliability, atomistic simulations, nano-device

In this paper, the impact of copper and oxygen vacancy balance in filament composition as a key factor for oxide-based CBRAM (Hybrid RRAM) performances is investigated. To this aim, several RRAM technologies are studied using various resistive layers and top electrodes. Material analyses allow to highlight the hybrid aspect of HRRAM conductive filament. Density functional theory simulations are used to extract microscopic features and highlight differences from a material point of view. Integrated RRAM technology performances such as window margin, endurance and retention are then measured to analyze copper and oxygen vacancy influence on device characteristics. A new RRAM classification correlating filament composition and memory performances is proposed.

1. Introduction

Post-CMOS alternative technologies are becoming critical for chip industry. Recently, alternative emerging technologies have gained interest targeting new applications as embedded device market, new computer architecture paradigms or flash memory replacement. Resistive random access memories (RRAM) performances such as high scalability,[1] fast

switching speed [2] and good endurance [3] make them potential candidates for standalone storage class or embedded memory.[4-6] Today, even flash memory has not been able to combine all of these features, especially in terms of writing speed. Furthermore, scaling down to nanoscale size requires switching currents in the order of tens of µA with more critical minimal dimensions. For the former, studies have shown the ability of RRAM to operate at sub-µA,[7] while novel integration solutions such as passive crossbars[8] and 3D stacking have been proposed to overcome the latter and to achieve extremely high packing density.[9] The understanding of switching mechanisms at device level is a key factor for a technology to be viable at very large scale integration. Different types of resistive memory devices have been studied in the past years such as oxide based memories (OxRAM) and conductive bridge memories (CBRAM). It should be noted that for both technologies it is very challenging to combine good cycling endurance, stable retention and high Window Margin (WM). Two distinct resistive states can be obtained based on a reversible filament formation (SET operation) and rupture (RESET operation) inside an insulating layer sandwiched between two electrodes; SET operation being the switching from a high resistive state (HRS) to a low resistive state (LRS) and RESET the reverse operation (HRS to LRS). In the case of CBRAM, metal ions coming from top electrode (TE) are introduced in the insulating layer. Working principle is based on a metallic filament formation and dissolution controlling performances.[10] These devices present high WM, relatively low endurance and poor retention stability.[11,12] In the case of OxRAM, oxygen vacancies creation and annihilation inside the oxide dominates the switching mechanism.[13-15] This technology shows low WM combined to high endurance and stable retention.[3,16] While lots of effort have been done lately to improve switching speed and power consumption in RRAM,[17,18] several challenges need to be overcome, namely the high extrinsic (device to device) and intrinsic (cycle to cycle) variability in RRAM characteristics.[7] High WM could potentially help solving this variability by maximizing the ratio of HRS over LRS. Moreover, coupling high WM and high

endurance (up to 10^8 cycles required for storage class applications[19]) remains a critical issue. Combining CBRAM and OxRAM in one hybrid oxide-based CBRAM (HRRAM) where filament can be composed of metal ions and oxygen vacancies could offer alternative performances such as high WM coupled with high endurance. Recent studies have identified materials issues in oxide and metal based RRAM.[20,21] However, material properties study is still lacking in HRRAM to guide stack choice (oxide vs electrodes) towards a given application. In a previous work, a trade-off between endurance, window margin and retention was demonstrated. When comparing various HRRAM electrical performances and filament composition, it appeared that material properties such as energy migration barrier of species composing switching filament is linked to HRRAM behavior.[22] It has been shown that oxygen vacancies formation is needed to introduce top electrode metal ions in different oxides.[23-26] Nevertheless, to our knowledge, the equilibrium between metal ions and oxygen vacancies dependence on the chosen material and its impact on device performances has never been investigated. Our study focuses on oxide/CuTeGe-based HRRAM, where Cu-rich based conductive filament controls the switching mechanism inside an oxide insulating layer.[17,27,28] In this work, the hybrid aspect of the conductive filament (composed of both Cu atoms and oxygen vacancies) is demonstrated based on Time of Flight Secondary Ion Mass Spectrometry profiles (ToF-SIMS). Afterward, filament composition is analyzed for various HRRAM technologies based on Density Functional Theory (DFT). To this aim, thermodynamic (based on defect formation enthalpy) and kinetics (based on defects migration energy) considerations are made. HRRAM devices are characterized to analyze typical performances such as WM, retention and endurance. Based on our simulations and experimental results, a comparison between different stacks exposes the impact of the balance between copper and oxygen vacancies on HRRAM performances, allowing us to propose a new HRRAM classification.

2. Technological Details

In this study, various RRAM technologies are investigated. The devices are integrated in 1T1R configuration using 130 nm CMOS transistor as selector. Memory stack is deposited following bottom electrode (BE)/switching material/top electrode (TE) structure. 5 nm of amorphous a-HfO_2,[26] 3 nm of amorphous a-Al_2O_3,[29] 4 nm of GdO_x,[30] and 10 nm of Ta_2O_5 were deposited by PVD or ALD on different PVD BEs (titanium nitride-TiN and tungsten W). 20 nm of $CuTe_xGe_y$ or 5 nm of Ti deposited by PVD was used as TE for HRRAM and OxRAM respectively. For the sake of comparison, a typical CBRAM (Ag/GeS_2)[11] is introduced in **Figure 1**. It has been demonstrated that Te and Ge are not involved in filament composition.[29] Ge is used to stabilize CuTe layer and to keep it amorphous during integration process, to prevent any segregation and phase separation. Typically, 10-20% Ge is used[31,32] in CuTe alloys. Moreover, CuTe bound is polar and can easily be broken in $Cu^{\delta+}$ and $Te^{\gamma-}$ ions. Due to its high formation energy compared to Cu, Te plays no role in the filament formation. Thus, only Cu ions are mobile under electric field. Consequently, in the following, HfO_2/Cu, Al_2O_3/Cu, Ta_2O_5/Cu and GdO_x/Cu will refer to HfO_2/$CuTe_xGe_y$, Al_2O_3/$CuTe_xGe_y$, Ta_2O_5/ $CuTe_xGe_y$ and GdO_x/$CuTe_xGe_y$ stacks respectively.

3. Hybrid Filament in HRRAM

3.1. ToF-SIMS Measurements

As indicated above, HRRAM is a device where both metallic ions and oxygen vacancies contribute to switching mechanism. Since a direct microscopic observation of an oxygen vacancy based filament at nanoscale level is still challenging, here we propose an indirect method based on Tof-SIMS measurements; a technique based on sputtering a surface with a focused ion beam and collecting ejected secondary ions. Spectra of copper and oxygen profiles versus sputtering time in HRS and LRS are presented in **Figure 2.a and b** for Ta_2O_5/Cu technology. In LRS state, Cu intensity in the $CuTe_2Ge$ region decreases (indicated

as less Cu in Figure 2.a). An increase of intensity is also observed in the signal incoming from the Ta_2O_5 region (indicated as more Cu in Figure 2.a). The copper content shift toward longer sputtering times corresponds to copper diffusion from the ion source layer (top electrode) toward the bottom electrode. This copper diffusion is consistent with a CBRAM behavior. On the other hand, when comparing LRS to HRS of oxygen profile in Figure 2.b, LRS state profile shows a decrease of oxygen content in the dielectric. Moreover, an increase of oxygen content is also observed in the $CuTe_2Ge$ region. This oxygen content shift corresponds to an oxygen diffusion toward the surface, leading to oxygen vacancies formation in the oxide as represented in Figure 2.c. This oxygen diffusion is consistent with OxRAM behavior. It is worth highlighting that as the ionization yield depends of the atomic environment of the element, when studying a stack of several layers, some matrix effects can appear at the interfaces. Moreover, during the sputtering some atoms can be repelled in the sub layers, thus in the spectra represented in Figure 2.a and b the interfaces positions are roughly estimated. As observed, both copper and oxygen profiles evolve when an external bias is applied. This behavior is associated to a hybrid behavior between pure CBRAM, where the filament is mainly composed of diffused metal and pure OxRAM where the filament is made of a path of local oxygen deficiencies namely vacancies. This hybrid mechanism is strongly correlated between vacancies and copper. Oxygen vacancies formed in the oxide weaken the chemical barrier properties, which eases copper diffusion. Stated differently, copper can easily follow paths formed by the organization of vacancies in the dielectric, in particular vacancies can be filled by copper atoms.

3.2. Atomistic Simulations

In order to give insight on microscopic mechanisms that could occur in all our integrated devices (HfO_2/Cu, Ta_2O_5/Cu, Al_2O_3/Cu and GdO_x/Cu), atomistic simulations were performed. Combining defect formation enthalpy (ΔH) and migration energy barrier (E_a), the most favorable defects that could compose a filament can be extracted. ΔH is the total energy

difference between an initial and a final state (introducing a new defect) representing an event between the oxide and the TE. E_a is the energy needed for a defect to diffuse in the oxide. The lower these values are, the more favorable the associated event is.

Table 1 summarizes the results. It can be noted, as seen in our calculations, that oxygen vacancy's formation is required to form the filament. Δ*H* of copper interstitial next to Oxygen vacancy site (Cu_iV_O) represents the lowest values in all cases validating the hybrid aspect of the formed filament. On the other hand, Δ*H* and E_a of V_O in HfO_2 and Ta_2O_5 are lower than in Al_2O_3 and GdO_x. Consequently, two filament features representing two different types of HRRAM could be identified: HRRAM where only Cu_iV_O defect is moving during memory operation, and HRRAM where both Cu_iV_O and V_O are moving. In HfO_2, Cu_iV_O introduction in the oxide are more favorable (Δ*H* and E_a lower) than copper interstitial (Cu_i). Thus, filament in HfO_2 could mainly be composed of V_O and Cu_iV_O. In the case of Ta_2O_5, Cu_i has a lower Δ*H* than V_O, nevertheless, it is easier to introduce and remove Cu_i when it is associated to V_O (Δ*H* Cu_iV_O =0.5eV). While Δ*H* of V_O is relatively high, it is combined to low migration energy, making it favorable to diffuse. Thus, in Ta_2O_5 the switching mechanism involves all of these studied defects. On the other hand, in Al_2O_3 and GdO_x, Cu_iV_O introduction in the oxide is the most favorable defect (Δ*H* in the order of 0.6eV vs 3.8eV for V_O in Al_2O_3 and 1.2eV vs 4.1eV for V_O in GdO_x). Moreover, by introducing aluminum atoms in GdO_x structure, Δ*H* Cu_iV_O is further reduced leading to a similar behavior as in Al_2O_3. Although V_O are necessary in HRRAM filament composition, they are either as favorable as Cu_iV_O defect (as in HfO_2) or less favorable (as in Al_2O_3 and GdO_x). In the case of Al_2O_3 and GdO_x, once V_O are created to introduce Cu ions during filament formation, Cu_iV_O are more favorable to be the core of switching mechanism at the expense of V_O. However, in HfO_2 and Ta_2O_5 both Cu_iV_O and V_O defects can participate to filament formation and disruption. Indeed in Ta_2O_5, Δ*H* V_O is higher than Δ*H* Cu_i, but is coupled to a very low migration energy making its diffusion favorable. **Figure 3.a and b** show the diffusion barrier of Cu_i, V_O, and (Cu_iV_O)

between two sites in Al_2O_3 and HfO_2 respectively; Al_2O_3/Cu and HfO_2/Cu being two devices with different filament features. As we can clearly see, in the case of Al_2O_3/Cu, (Cu_iV_O) is the most favorable to be introduced and removed in the filament. On the other hand, in the case of HfO_2, both V_O and (Cu_iV_O) are favorable compared to Cu_i.

4. HRRAM Classification versus Performances

It has been shown that during cycling, non-reversible defect generation gradually degrades the oxide leading to device failure when the maximum number of cycles is reached.[26,33,34] Consequently, limiting non-reversible defect generation is a key to improve endurance. Based on our simulation results, different types of filament are identified. Although V_O are required to favor Cu insertion leading to a hybrid filament, V_O can become hard to remove and be source of defect generation eventually leading to oxide degradation as in GdO_x/Cu. In a material where Cu_iV_O are more favorable than V_O, switching filament is richer in Cu. However, the energy required to remove the small amount of V_O is higher than for removing Cu_iV_O. To remove V_O, higher energy should be provided to the oxide, leading to higher defect generation. Moreover, favoring further Cu_iV_O at the expense of V_O as in GdO_x-Al/Cu and Al_2O_3/Cu leads to a hybrid filament with less V_O in its vicinity. In this case, the generation of non-reversible defects decreases leading to higher endurance. As completely removing V_O from filament formation cannot be considered to decrease defect generation, V_O need to be easily removed to improve endurance. This can be obtained by adjusting Cu_iV_O /V_O balance. In particular, when V_O and Cu_iV_O have the same occurrence probability in SET and RESET operations, they both participate to filament formation and disruption. V_O and Cu_iV_O are thus easily recovered during RESET, leading to low defect generation and good endurance. It can be noted that if migration energy barrier of both species is high, endurance will be degraded due to the high required energy to switch the memory.[33]

Based on these results, Two groups of HRRAM can be identified as presented in **Figure 4**: 1) Cu_iV_O is favored at the expense of V_O leading to difficult V_O recovery and earlier oxide degradation (lower endurance). 2) V_O as favorable as Cu_iV_O to be removed leads to a V_O easy to recover and thus low defect generation (high endurance). It can be noted that in the case of V_O becoming more favorable than Cu_iV_O, the filament is no longer considered as hybrid and is mainly composed of V_O, leading to OxRAM behavior.

The impact of filament composition on device performances is shown in **Figure 5**. In order to compare device performances, three different features could be evaluated: window margin being the ratio between HRS and LRS, endurance being the maximum of SET/RESET cycles a cell can reach before final failure (oxide breakdown) and retention representing the temperature stability over time. These characteristics are interdependent; improving two features leads to the degradation of the third one. In particular, increasing WM and endurance degrades retention. Here, we compare the best endurance that could be reached for various integrated technologies and we correlate the results with filament composition. Figure 5.a illustrates WM evolution with cycling endurance. Experimental results comply with HRRAM classification based on atomistic simulations (Figure 4). Red and blue colors represent devices with TiN and W as bottom electrode respectively. Endurance is lower in Al_2O_3/Cu and GdO_x/Cu than in HfO_2/Cu (details in supplementary material). Adjusting V_O and Cu_iV_O competition in the filament leads to different performances. If V_O is as favorable as Cu_iV_O to be introduced and diffused during SET and RESET (HfO_2/Cu), endurance is improved. If V_O is less favorable (Al_2O_3/Cu and GdO_x/Cu), endurance is degraded. In the latter, V_O presence, needed to introduce Cu in the oxide, are less favorable compared to Cu_iV_O. These samples present an early oxide degradation (lower endurance). Comparing Al_2O_3 and GdO_x where Cu_iV_O dominates the switching mechanism, GdO_x has a lower endurance than Al_2O_3. This can be due to a lower defect enthalpy and energy migration barrier (0.6 vs 1.2 eV for ΔH and 1.4 vs 3.44 eV for E_a). As previously seen, by introducing Al in GdO_x structure, Cu_iV_O ΔH is

further reduced leading to a comparable filament composition as in Al_2O_3. This is confirmed in Figure 5.a: by doping GdO_x with aluminum, endurance is improved and tends toward Al_2O_3. Combining endurance results and atomistic calculations, it appears that Al presence in the oxide favors Cu insertion next to V_O. An OxRAM and a CBRAM are introduced in Figure 5 for comparison sakes.

Consequently, in a material where Cu_iV_O is more favorable than V_O, favoring further Cu_iV_O increases the endurance. In other words, improving Cu insertion leads to a filament easier to form and disrupt during SET and RESET, leading to a better endurance regardless WM. Figure 5.b and c represent the comparison between best case and worst case for endurance and data retention respectively. In figure 5.b, endurance of HfO_2/Cu (6.10^9 cycles) is compared to GdO_x (where only 10^3 cycles can be reached). On the other hand, in Figure 5.c, temperature stability of the same devices in Figure 5.b is compared at 200°C. As clearly seen, the higher the endurance is, the lower the retention is. One should note that endurance performances are not only related to the hybrid character of the RRAM, but are also linked to the respective V_O, Cu and Cu_iV_O energy costs. Moreover, the highest endurance/WM tradeoff is due to the use of a tungsten based bottom electrode which favors the RESET due to tungsten high thermal conductivity favoring thermal dissipation. Thus, the energy needed to RESET the device is lowered. These conditions favor the cycling capacities of the device at the expense of the temperature stability as shown in figure S2.b.

To further investigate the difference between the two filament features presented above, we have studied forming operation with two different polarizations in HfO_2/Cu and Al_2O_3/Cu (more details in supplementary materials). Figure S.5 represents the time to breakdown t_{BD} versus forming voltage (V_f). For HfO_2/Cu, t_{BD} and V_f are similar in both polarizations. In the case of Al_2O_3/Cu, higher forming voltage is observed for short t_{BD} when TE is negatively polarized preventing Cu insertion in the oxide. HfO_2/Cu shows similar switching mechanism in both polarizations while Al_2O_3/Cu exposes different working principle depending on

polarization. In HfO_2, The conductive filament formation with Cu_iV_O or only V_O has no impact on t_{BD}. In Al_2O_3, as the introduction of copper is more favorable than oxygen vacancies, its introduction in direct forming eases filament formation and lower forming voltage.

Consequently, we present a panel of filament composition to be aimed depending on the targeted application. CBRAMs present high WM while OxRAMs show high endurance and stable retention. Combining OxRAM and CBRAM in one hybrid HRRAM, performance compromises could be achieved. Large WM and high endurance are obtained in HfO_2/Cu owing to V_O/Cu_iV_O equilibrium in the switching filament. On the other hand, large WM and stable retention could be achieved due to favoring Cu_iV_O at the expense of V_O as in GdO_x/Cu and Al_2O_3/Cu.

5. Conclusion

In this work, the impact of balancing metal ions and oxygen vacancies in HRRAM filament on device performances was investigated. Filament composition was studied by first principle calculations and maximum endurance was identified for different HRRAM. Combining experimental results and atomistic simulations, we highlighted filament features to improve endurance characteristics. In particular, we demonstrated that in HRRAM, V_O are necessary to form a Cu-rich filament. The switching mechanism is thus controlled by Cu ions and Oxygen vacancies. However, two types of filament were put in evidence. Filament where Cu_iV_O are more favorable to control switching mechanism at the expense of V_O (Al_2O_3 and GdO_x) presents V_O hard to be recovered leading to early oxide degradation (low endurance). Decreasing Cu_iV_O formation enthalpy and diffusion barrier in oxide leads to filament richer in Cu_iV_O (poorer in V_O) and improves endurance. However, V_O need to be easily removed during RESET to further improve endurance. This can be obtained by adjusting Cu_iV_O /V_O balance (V_O as favorable as Cu_iV_O to be introduced and removed from oxide). In this case,

both defects participate in filament formation and disruption. V_O and Cu_iV_O are thus easily recovered leading to low defect generation (higher endurance as in HfO_2/Cu). In summary, we presented a panel of filament composition, giving insights to choose the most suitable technology (RRAM resistive layer and electrodes) for a given application with required specifications.

Acknowledgements
This work has been partially supported by the European 621217 PANACHE project.
"Gilbert Sassine and Cécile Nail contributed equally to this work."
This work was supported by the H2020 WakeMeUp project.
Received: ((will be filled in by the editorial staff))
Revised: ((will be filled in by the editorial staff))
Published online: ((will be filled in by the editorial staff))

References

[1] B. Govoreanu, G. S. Kar, Y-Y. Chen, V. Paraschiv, S. Kubicek, A. Fantini, I. P. Radu, L. Goux, S. Clima, R. Degraeve, N. Jossart, O. Richard, T. Vandeweyer, K. Seo, P. Hendrickx, G. Pourtois, H. Bender, L. Altimime, D. J. Wouters, J. A. Kittl, M. Jurczak, 2011 International Electron Devices Meeting, Washington DC, **2011**, 31.6.1.

[2] A. C. Torrezan, J. P. Strachan, G. Medeiros-Ribeiro, R. S. Williams, *Nanotechnology* **2011**, *22*, 485203.

[3] M-J. Lee, C. B. Lee, D. Lee, S. R. Lee, M. Chang, J. H. Hur, Y-B. Kim, C-J. Kim, D. H. Seo, S. Seo, U-I. Chung, I-K. Yoo, K. Kim, *Nature Materials* **2011**, *10*, 625.

[4] S. Sills, S. Yasuda, J. Strand, A. Calderoni, K. Aratani, A. Johnson, N. Ramaswamy, 2014 Symposium on VLSI Technology (VLSI-Technology): Digest of Technical Papers, Honolulu, **2014**, 1.

[5] J.R. Jameson, P. Blanchard, C. Cheng, J. Dinh, A. Gallo, V. Gopalakrishnan, C. Gopalan, B. Guichet, S. Hsu, D. Kamalanathan, D. Kim, F. Koushan, M. Kwan, K. Law, D. Lewis, Y. Ma, V. McCaffrey, S. Park, S. Puthenthermadam, E. Runnion, J. Sanchez, J. Shields, K. Tsai, A. Tysdal, D. Wang, R. Williams, M.N. Kozicki, J. Wang, V. Gopinath, S. Hollmer,

M. Van Buskirk, 2013 IEEE International Electron Devices Meeting, Washington DC, **2013**, 30.1.1.

[6] Z. Wei, K. Eriguchi, S. Muraoka, K. Katayama, R. Yasuhara, K. Kawai, Y. Ikeda, M. Yoshimura, Y. Hayakawa, K. Shimakawa, T. Mikawa, S. Yoneda, 2015 IEEE International Electron Devices Meeting (IEDM), Washington DC, **2015**, 7.7.1.

[7] A. Fantini, L. Goux , R. Degraeve , D.J. Wouters, N. Raghavan , G. Kar , A. Belmonte, Y.-Y. Chen, B. Govoreanu , M. Jurczak, *2*013 5th IEEE International Memory Workshop, Monterey CA, **2013**, 30.

[8] M. Prezioso, F. Merrikh-Bayat, B. D. Hoskins, G. C. Adam, K. K. Likharev, D. B. Strukov, *Nature* **2011**, *521*, 61.

[9] Y. Bai, H. Wu, K. Wang, R. Wu, L. Song, T. Li, J. Wang, Z. Yu, H. Qian, *Scientific Reports* **2015**, *5*, 13785.

[10] I. Valov, R. Waser, J. R. Jameson, M. N Kozicki, *Nanotechnology* **2011**, *22*, 289502.

[11] E. Vianello, C. Cagli, G. Molas, E. Souchier, P. Blaise, C. Carabasse, G. Rodriguez, V. Jousseaume, B. De Salvo, F. Longnos, F. Dahmani, P. Verrier, D. Bretegnier, J. Liebault, 2012 Proceedings of the European Solid-State Device Research Conference (ESSDERC), Bordeaux, **2012**, 278.

[12] S. Pi, M. G. Sadrabadi, J. C. Bardin, Q. Xia, *Nature Communication* **2015**, *6*, 7519.

[13] D. B. Strukov, G. S. Snider, D. R. Stewart, R. S. Williams, *Nature*, **2009**, *459*, 1154.

[14] J. J. Yang, D. B. Strukov, D. R. Stewart, *Nature Nanotechnology*, **2013**, *8*, 13.

[15] G. Sassine, S. La barbera, N. Najjari, M. Minvielle, C. Dubourdieu, F. Alibart, *Journal of Vacuum Science & Technology B, Nanotechnology and Microelectronics: Materials, Processing, Measurement, and Phenomena*, **2016**, *34*, 012202-1.

[16] T-C. Chang, K-C. Chang, T-M. Tsai, T-J. Chu, S. M. Sze, *Materials Today*, **2016**, *19*, 254.

[17] S. Menzel, U. Böttger, M. Wimmer, M. Salinga, *Adv. Funct. Mater.* **2015**, *25*, 6306.

[18] G. Sassine, C. Cagli, J. Nodin, G. Molas and E. Nowak, *IEEE Journal of the Electron Devices Society*, **2018**, *6*, 696.

[19] ITRS, "Executive Report," http://www.itrs2.net/, accessed: 2015.

[20] L. Zhu, J. Zhou, Z. Guo, Z. Sun, *J Materiomics*, **2015**, *1*, 285.

[21] J. Shang, G. Liu, H. Yang, X. Zhu, X. Chen, H. Tan, B. Hu, L. Pan, W. Xue, R-W. Li, *Adv. Funct. Mater.* **2014**, *24*, 2171.

[22] C. Nail, G. Molas, P. Blaise, B. Sklenard, R. Berthier, M. Bernard, L. Perniola, G. Ghibaudo, C. Vallée, *IEEE Transactions on Electron Devices*, **2017**, *64*, 4479.

[23] R. Waser, R. Dittmann, G. Staikov, Kristof Szot, *Adv. Mater.* **2009**, *21*, 2632.

[24] M. Saadi, P. Gonon, C. Vallée, C. Mannequin, H. Grampeix, E. Jalaguier, F. Jomni, A. Bsiesy, Journal of Applied Physics **2016**, *119*, 114501.

[25] G. Molas, E. Vianello, F. Dahmani, M. Barci, P. Blaise, J. Guy, A. Toffoli, M. Bernard, A. Roule, F. Pierre, C. Licitra, B. De Salvo, L. Perniola, *2014 IEEE International Electron Devices Meeting*, San Francisco CA, **2014**, 6.1.1.

[26] C. Nail, G. Molas, P. Blaise, G. Piccolboni, B. Sklenard, C. Cagli, M. Bernard, A. Roule, M. Azzaz, E. Vianello, C. Carabasse, R. Berthier, D. Cooper, C. Pelissier, T. Magis, G. Ghibaudo, C. Vallée, D. Bedeau, O. Mosendz, B. De Salvo, L. Perniola, *2016 IEEE International Electron Devices Meeting (IEDM)*, San Francisco CA, **2016**, 4.5.1.

[27] U. Celano, L. Goux, A. Belmonte, K. Opsomer, A. Franquet, A. Schulze, C. Detavernier, O. Richard, H. Bender, M. Jurczak, W. Vandervorst, *Nano Lett.* **2014**, *14*, 2401.

[28] D. S. Jeong, R. Thomas, R. S. Katiyar, J. F. Scott, H. Kohlstedt, A. Petraru, C. S. Hwang, *Rep. Prog. Phys.* **2012**, *75*, 076502.

[29] C. Nail, P. Blaise, G. Molas, M. Bernard, A. Roule, A. Toffoli, L. Perniola, C. Vallée, *Journal of Applied Physics*, **2017**, *122*, 024503.

[30] M. Barci, J. Guy, G.Molas, E. Vianello, A. Toffoli, J. Cluzel, A. Roule, M. Bernard, C. Sabbione, L. Perniola, B. De Salvo, *2014 IEEE International Reliability Physics Symposium*, Waikoloa HI, **2014**, 5E.3.1.

[31] W. Devulder, K. Opsomer, M. Jurczak, L. Goux and C. Detavernier, *2015 IEEE International Interconnect Technology Conference and 2015 IEEE Materials for Advanced Metallization Conference (IITC/MAM)*, Grenoble, **2015**, 215.

[32] K. Ohba, S. Yasuda, T. Mizuguchi, K. Aratani, M. Shimuta, A. Kouchiyama, M.Ogasawara (Sony Semiconductor Solutions Corp), US 13018744, **2011**.

[33] S. Balatti, S. Ambrogio, Z.-Q. Wang, S. Sills, A. Calderoni, N. Ramaswamy, D. Ielmini, *2014 IEEE International Electron Devices Meeting*, San Francisco CA, **2014**, 14.3.1.

[34] G. Sassine, D. Alfaro Robayo, C. Nail, J.-F. Nodin, J. Coignus, G. Molas, E. Nowak, *2018 IEEE International Memory Workshop (IMW)*, Kyoto, **2018**, 1.

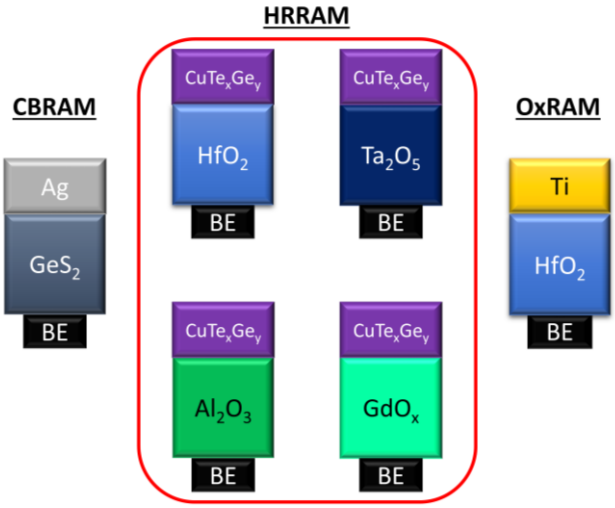


Figure 1. Schematics of RRAM stacks studied in this work. In HRRAM, switching mechanism is controlled by hybrid filaments composed of both Cu and V_O species.

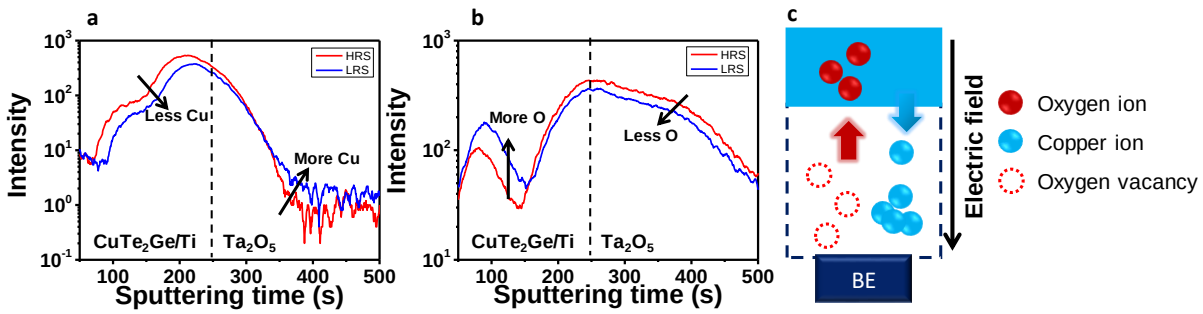


Figure 2. ToF-SIMS profiles. (a) and (b) copper and oxygen ToF-SIMS profiles in HRS (red lines) and LRS (blue lines) for Ta_2O_5/Cu memory. In LRS state, Cu intensity in the $CuTe_2Ge$/Ti region decreases, and increases in Ta_2O_5 region. Inversely, Oxygen decreases in Ta_2O_5 and increases in $CuTe_2Ge$/Ti leading to V_O formation in Ta_2O_5. These profiles illustrate hybrid composition of the conductive filament in HRRAM. (c) Schematic representation of oxygen and copper ions diffusion under external bias.

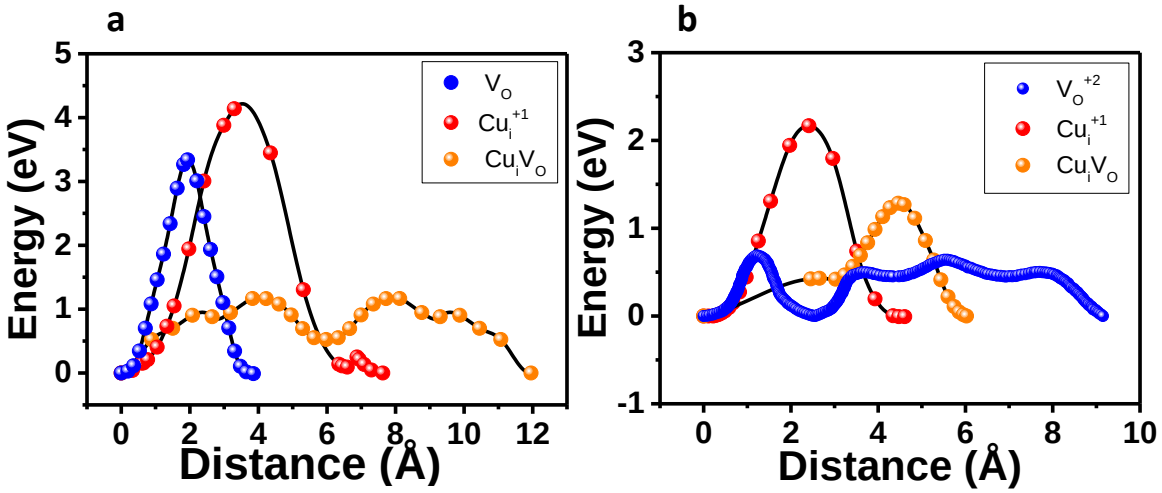


Figure 3. Migration barrier of V_O, Cu_i and Cu_iV_O between two sites in (a) Al_2O_3/Cu and (b) HfO_2/Cu respectively. In Al_2O_3, diffusion of Cu_iV_O is the most favorable event. On the other hand, in the case of HfO_2, Cu_iV_O and V_O are favorable to diffuse.

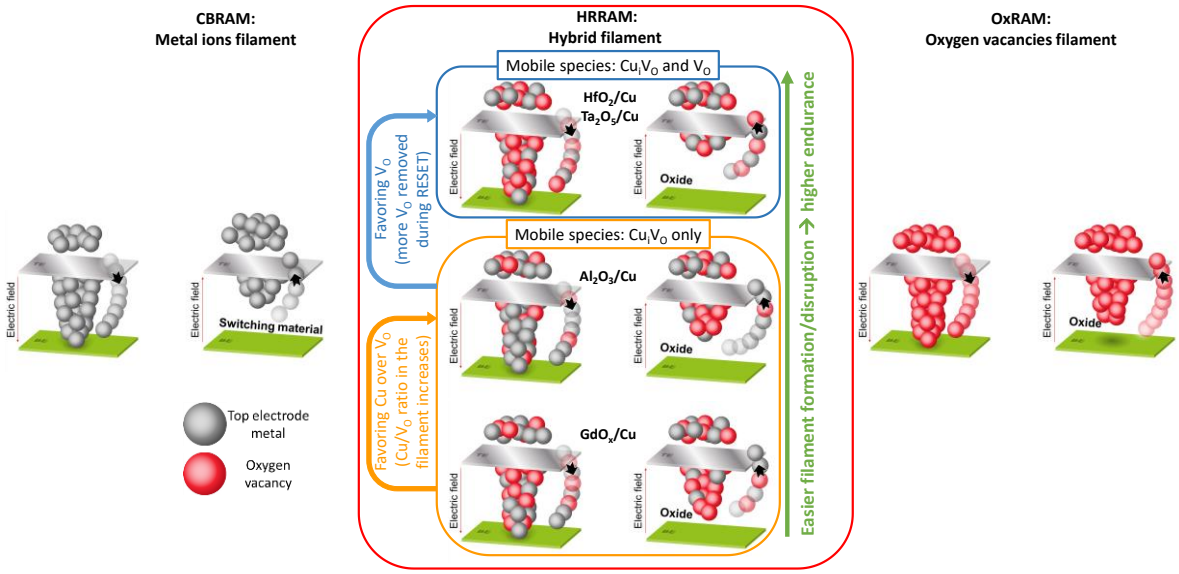


Figure 4. Schematics of filament formation and disruption in different RRAM technologies. CBRAM (left) working principle relies on metal ions, coming from the top electrode,

introduction in a switching layer while OxRAM (right) relies on oxygen vacancies formation. Summary of HRRAM filament composition depending on switching materials. Filament is composed of oxygen vacancy (V_O) and copper introduced next to V_O (Cu_iV_O). Two HRRAM groups could be distinguished depending on filament composition: 1) Cu_iV_O is favored at the expense of V_O leading to V_O hard to be recovered and low endurance (in orange frame). 2) V_O as favorable as Cu_iV_O to be removed leads to a V_O easy to recover and thus high endurance (in blue frame). In the first group, V_O is still necessary to form the filament but it is harder to remove than Cu_iV_O. Group 1 presents thus earlier oxide degradation leading to a low endurance. However, favoring Cu_iV_O by decreasing its formation enthalpy and migration energy barrier improves endurance (Al_2O_3/Cu versus GdO_x/Cu). To further improve endurance, equilibrium between V_O and Cu_iV_O is necessary (group 2). Formation enthalpy and migration energy barrier for both species become of the same order of magnitude leading to filament formation and disruption at a low energy budget.

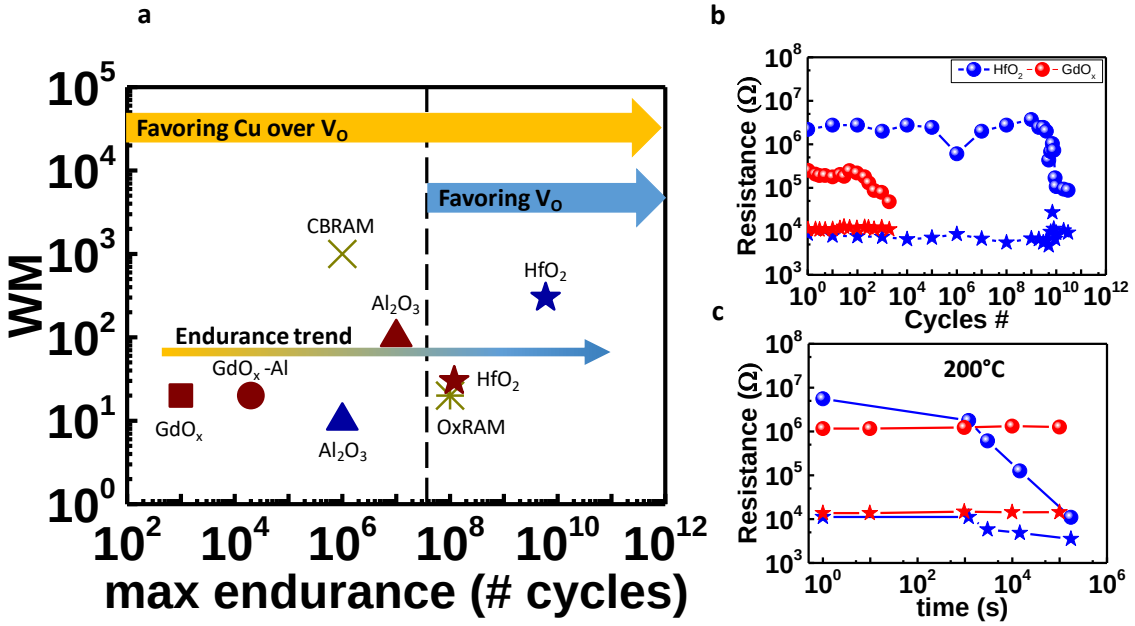


Figure 5. (a) Maximum endurance reached for all studied materials. TiN bottom electrode in red and W in blue. Ag/GeS_2 CBRAM and HfO_2/Ti OxRAM are also presented. The black dashed line separates the two groups of HRRAM depending on their filament composition. On the left side, decreasing Cu_iV_O formation enthalpy and diffusion barrier in oxide improves endurance (left arrow). However, on the right side, having V_O formation enthalpy and diffusion barrier of the same order of magnitude as Cu_iV_O avoid early oxide degradation leading to a better endurance (blue arrow). Endurance trend depending on copper and oxygen vacancies balance in the switching filament composition regardless WM is presented. (b) and (c) comparison between best case and worst case for cycling endurance and data retention respectively.

Table 1. Migration energy barrier, E_a, and formation enthalpy, ΔH, between the top electrode and various oxides extracted from atomistic simulations. Parenthesis represent the charge of the mobile defect.

Defect [eV]	HfO_2		Ta_2O_5		Al_2O_3		GdO_x		GdO_x-Al
	ΔH	E_a	ΔH	E_a	ΔH	E_a	ΔH	E_a	ΔH
Cu_i^{1+}	3.4	2.5	1.3	X	2.5	4	3.2	2	3.6
V_O^x	2.5(+2)	0.7(+2)	2.4(+2)	0.38(+2)	3.8(0)	3.5(0)	<3.5(0)	X	<3.5(0)
$(Cu_iV_O)^{+1}$	2.6	1.3	0.5	X	0.6	1.4	1.3	3.44	-0.2
Filament		**V_O and Cu_i next to V_O**					**Cu_i next to V_O**		

Copyright WILEY-VCH Verlag GmbH & Co. KGaA, 69469 Weinheim, Germany, 2016.

Supporting Information

Title Hybrid-RRAM Towards Next Generation of Non-volatile Memory: Coupling of Oxygen Vacancies and Metal Ions

Author(s), and Corresponding Author(s) Gilbert Sassine*, Cécile Nail, Philippe Blaise, Benoit Sklenard, Mathieu Bernard, Rémy Gassilloud, Aurélie Marty, Marc Veillerot, Christophe Vallée, Etienne Nowak, and Gabriel Molas**

1. ToF-SIMS Measurements

ToF-SIMS measurements were done on Ta_2O_5/Cu based stack in HRS and LRS. The tested stack was as follows: Ta (200nm)/TiN (5nm)/Ta_2O_5 (10nm)/Ti (1nm)/$CuTe_2Ge$ (15nm)/TiN (5nm) as presented in **Figure S1.a.** For LRS a ramp voltage was applied with a compliance current fixed at $5x10^{-3}$ A (figureS1.b). Then a sputter guns with 500eV O_2 or Cs were used, with an ion detection mode with Bi^+ and Bi^{3+} ions at 25keV and a detection of positive ions in M^+, M^- and MCs^+ modes. ToF-SiMS spectra presented in Figure 2 in the main text show the diffusion of copper and from $CuTe_2Ge$/Ti toward Ta_2O_5 during SET operation. On the other hand, spectra shows diffusion of oxygen from the oxide toward top electrode forming oxygen vacancies in the vicinity of the dielectric.

2. Electrical Characterization

To study the technology choice impact on endurance, we compare the best endurance that could be reached for different stacks. First, we compare HfO_2/Cu based HRRAM with a typical HfO_2/Ti OxRAM to identify the impact of Cu presence in the switching filament on device characteristics. Then we identify different type of filament behavior by changing the switching material in memory stack. Four HRRAM cases are studied (HfO_2/Cu, Al_2O_3/Cu, GdO_x/Cu and GdO_x-Al/Cu).

2.1 HRRAM versus OxRAM

In order to identify Cu contribution in HRRAM, typical HfO_2/Ti OxRAM is compared with HfO_2/Cu HRRAM. **Figure S2.a and c** illustrate the maximum endurance that could be achieved for both technologies with two different bottom electrodes. In the case of tungsten BE, HRRAM presents higher maximum endurance as 6.10^9 cycles could be reached before degradation, versus 10^8 in OxRAM. In the case where TiN is used as BE, no clear effect is noticed. However, retention measurements show that OxRAM presents higher stability over time than HRRAM. For both BEs no resistance variation is observed after 24h at 200°C for HfO_2/Ti, while HRS failure (resistance drift towards lower values) is obtained in the case of HRRAM (figure S2.b and d). BE impact on device performance is not treated in this study. In a previous work [22] a trade-off between WM, endurance and retention can be found in HRRAM. Increasing WM and endurance in the case of W/HfO_2/Cu compared to W/HfO_2/Ti leads to a degraded retention (W BE is chosen as maximum endurance has been reached). This has been correlated to the energy migration barrier of the species composing the filament. Decreasing this energy leads to a degraded retention. It can be noted that a correlation with a typical CBRAM behavior can be made; Ag/GeS_2 presents high WM, a relatively high endurance and a poor retention due to the metallic filament feature [11]. Thus, the low retention stability of HfO_2/Cu could be due to Cu metal ions insertion into filament composition. Cu presence in the filament could be noticed as well by studying SET behavior in both technologies.

2.2 Copper Impact on Switching Behavior

In the aim of studying copper metal ions contribution in the oxide, a quasi-static voltage ramp is applied on 1T1R 4kbs memory arrays [18]. This method allows the measurement of switching voltage and switching time in a memory device. It consists in continuously increasing the applied voltage at different ramp rate until switching occurs (inset of **Figure S3**). The voltage stress is applied on HfO_2/Ti OxRAM and HfO_2/Cu HRRAM in both SET

(HRS to LRS) and RESET (LRS to HRS) respectively. Figure S3 represents switching time in logarithmic scale versus switching voltage. Based on a previews study[18] it was shown that in Ramped Voltage Stress the switching time effect is not cumulative. Consequently, the switching time is computed from the starting of the voltage step where the switching occurs. It can be noticed that when a positive voltage is applied on the top electrode (TE), a lower voltage is needed to SET HRRAM compared to OxRAM. However, the same behavior is observed in RESET for both HRRAM and OXRAM. In SET (positive voltage on the TE), copper ions insertion in the oxide favors the filament formation. Thus lower energy is required to SET the HRRAM.

2.3 HRRAM with Stable Retention

As Cu ions contribution to the filament formation was identified in HRRAM, different behavior are evaluated by changing switching material. In order to show its impact on endurance, Al_2O_3 and GdO_x known as typical materials for high retention are studied [29.30].

Figure S4.a and c show the retention stability of Al_2O_3/Cu with two different BEs (TiN and W) and TiN/GdO_x/Cu respectively. There is no resistance variation measured for both materials at 200°C. However, as shown in figure S4 b and d, where the best case of endurance are presented, Al_2O_3 and GdO_x show lower cycling endurance than HfO_2/Cu regardless of the chosen WM; $10^7$and 10^6 cycles are reached in the case of TiN/Al_2O_3/Cu (high WM) and W/Al_2O_3/Cu (low WM) respectively. In the case of GdO_x/Cu the maximum cycling endurance we could attain is at the order of 10^3. Trying to reach Al_2O_3 endurance characteristics, GdO_x has been doped with Aluminum (Al). An improvement in cycling endurance is noticed in GdO_x-Al/Cu compared to GdO_x/Cu as shown in figure S4 d. Figure S4 c shows no resistance variation at 200°C. In conclusion, regardless the chosen WM, Al_2O_3 and GdO_x cannot reach HfO_2/Cu performance in terms of endurance.

2.4 Forming Polarity

In this part, forming is studied in HfO_2/Cu and Al_2O_3/Cu HRRAM. Two different polarizations are applied using the quasi-static method presented above: direct forming where the forming voltage is applied on the top electrode and reverse forming where the forming voltage is applied on the bottom electrode. Direct forming implies Copper (Cu) and oxygen vacancies (V_O) formation in the vicinity of the oxide while in reverse forming, as Cu is positively polarized, its introduction in the oxide is thus not possible. In this case, only V_O formation is considered. In this study, **Figure S5** represents the time to breakdown t_{BD} vs V_{switch} for direct and reverse forming. For HfO_2/Cu, t_{BD} and V_{switch} are similar in direct and reverse forming. In the case of Al_2O_3/Cu, higher reverse forming voltage is observed for short t_{BD}. HfO_2/Cu shows similar switching mechanism in both polarizations while Al_2O_3/Cu exposes different working principle depending on polarization. In HfO_2/Cu, as V_O are as favorable as Cu_iV_O, no real impact of copper insertion on oxide breakdown is observed; same behavior is noticed in direct and reverse forming. However, in the case of Al_2O_3, where Cu_iV_O are more favorable than V_O, the filament formation requires lower voltage in direct forming where Cu_iV_O dominates the switching mechanism compared to reverse forming where only V_O controls the switching.

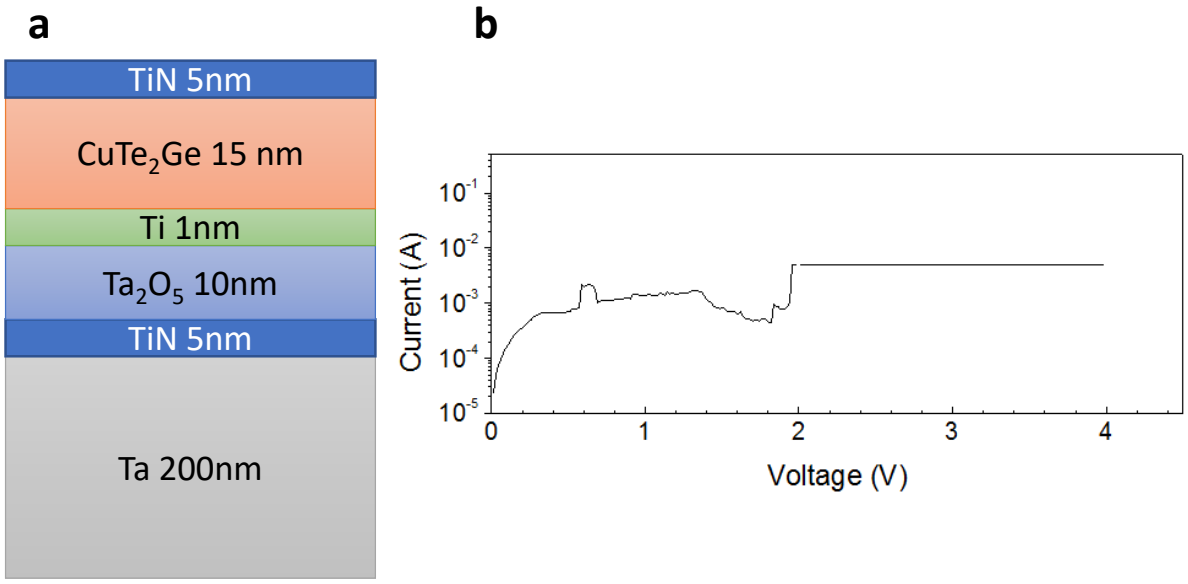


Figure S1. (a) studied stack in ToF-SIMS. (b) Current voltage characteristic of the studied device during SET operation.

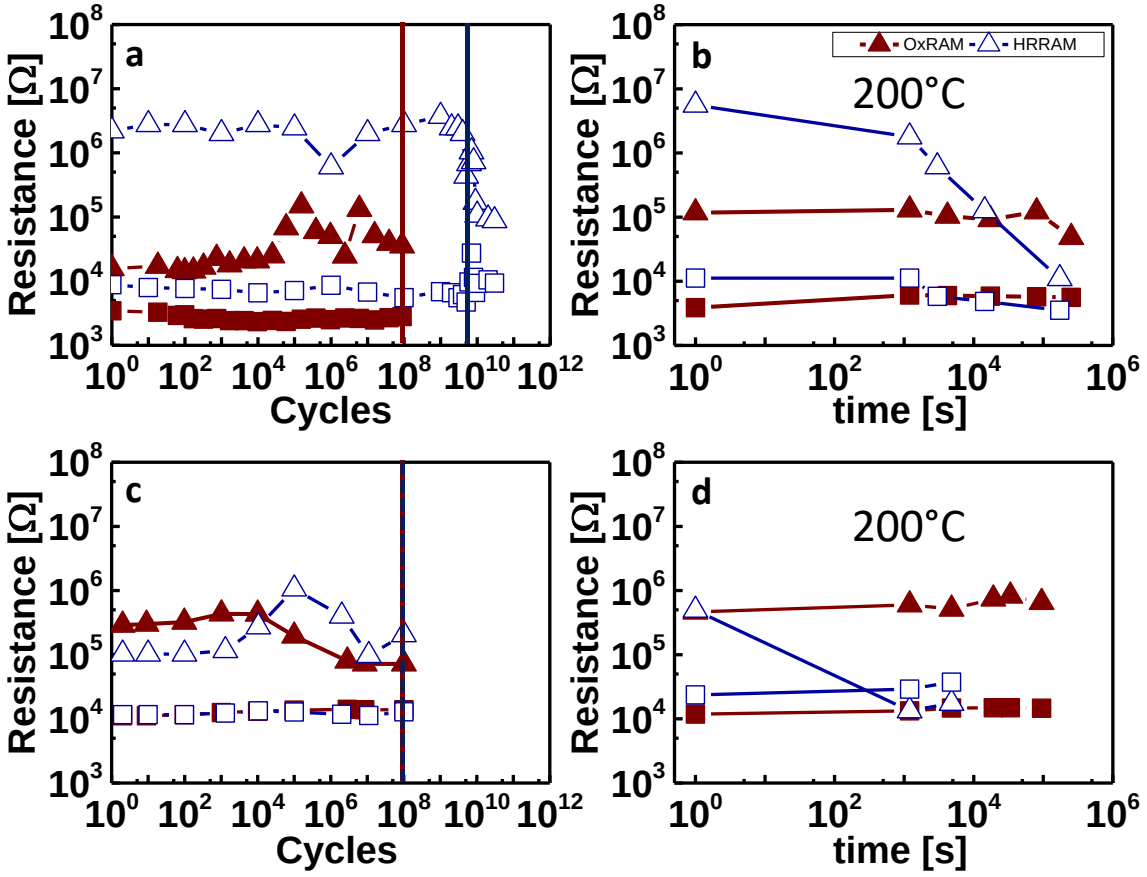


Figure S2. (a) Endurance and retention (at 200°C) measurement for (a), (b) W/HfO_2/Cu and W/HfO_2/Ti and (c), (d) TiN/HfO_2/Cu and TiN/HfO_2/Ti. In (a) and (c) lines designates the maximum number of cycles reached before filament degradation. In W/HfO_2/Cu 6 10^9 are reached versus 10^8 for W/HfO_2/Ti (a). As for TiN bottom electrodes (c), 10^8 could be reached for both OXRAM and HRRAM. 24 hours stability is reached for OxRAM (W and TiN BE) while HRS failure is clearly observed in HRRAM (b) and (d).

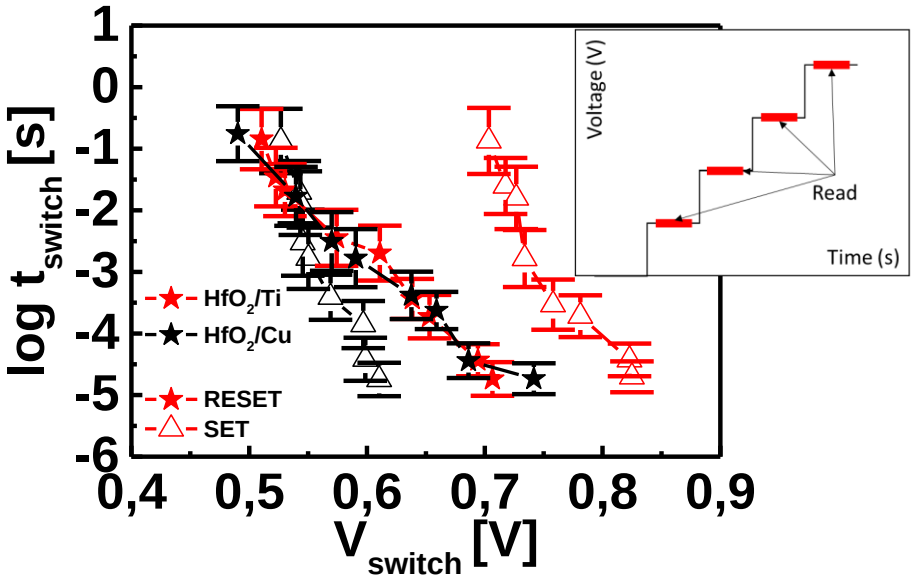


Figure S3. (a) t_{switch} versus V_{switch} in SET and RESET for HfO_2/Cu and HfO_2/Ti.

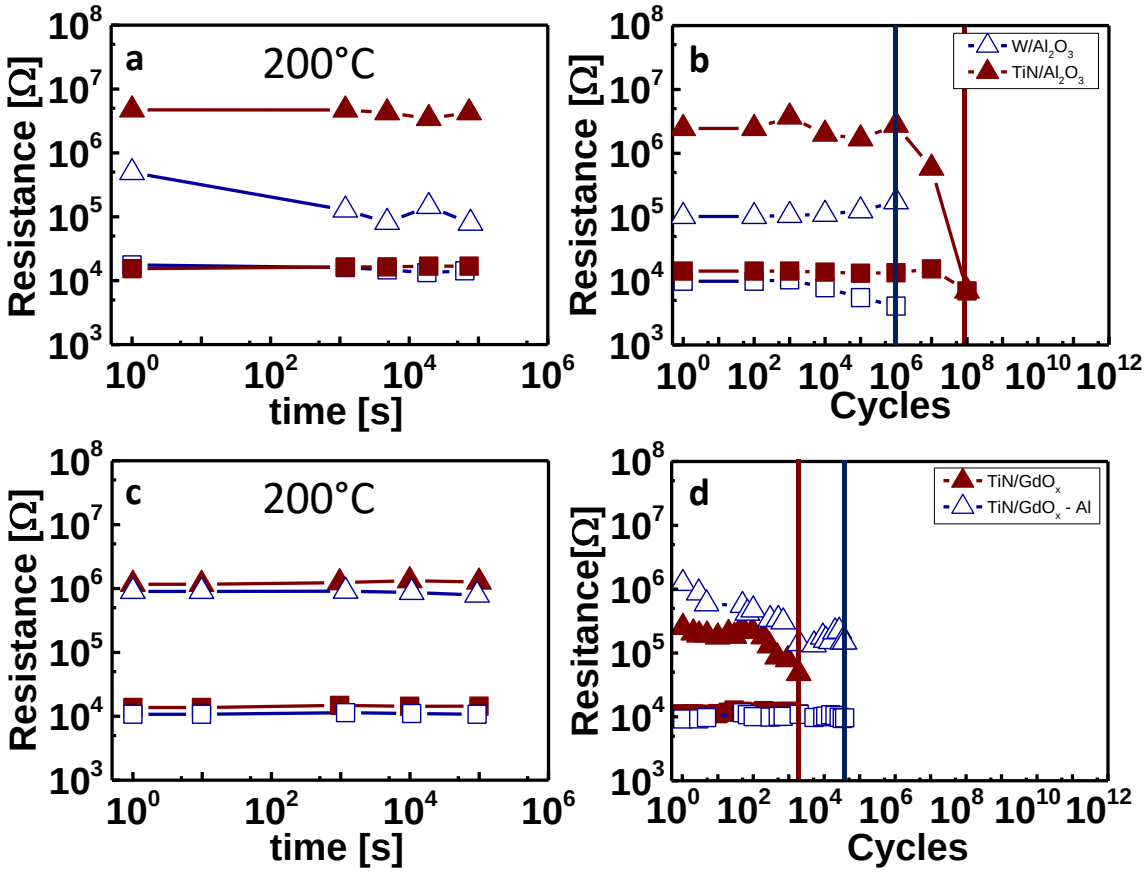


Figure S4. Retention at 200°C and endurance measurement for (a), (b) W/Al_2O_3/Cu and TiN/Al_2O_3/Cu. and (c), (d) TiN/GdO_x/Cu and TiN/GdO_x-Al/Cu. 24 hours stability is reached for all tested HRRAM devices (a) and (c). Lines designates the maximum number of cycles reached before filament degradation. In W/Al_2O_3/Cu 10^6 cycles are reached versus 10^7 cycles for TiN/Al_2O_3/Cu (b). As for GdO_x (d), 10^3 cycles are reached, whereas up to 5 10^4 cycles are obtained after Al doping.

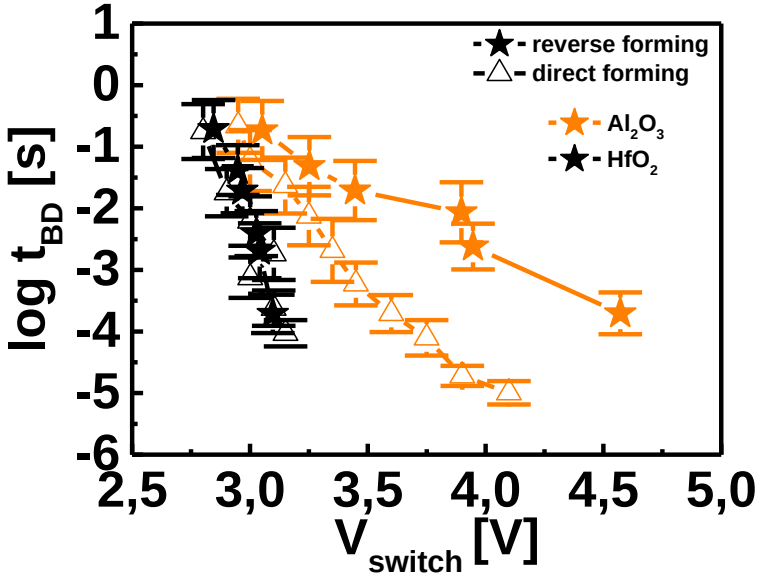


Figure S5. (a) t_{BD} versus forming voltage in direct and reverse polarity for HfO_2/Cu and Al_2O_3/Cu.